



High resolution liquid level sensor based on Archimedes' law of buoyancy using polymer optical fiber Bragg gratings

Cláudio C. Ramos^a, João Preizal^a, Xuehao Hu^b, Christophe Caucheteur^b, Getinet Woyessa^d, Ole Bang^d, Ana M. Rocha^c, Ricardo Oliveira^{a,*}

^a Instituto de Telecomunicações, University of Aveiro, Aveiro, Portugal

^b Department of Electromagnetism and Telecommunication, University of Mons, Boulevard Dolez 31, Mons 7000, Belgium

^c I3N and Physics Department, University of Aveiro, Aveiro, Portugal

^d DTU Electro, Department of Electrical and Photonics Engineering, Technical University of Denmark, 2800 Kgs. Lyngby, Denmark

ARTICLE INFO

Keywords:

Liquid level sensor
Fiber Bragg grating
Polymer optical fiber

ABSTRACT

In this paper, we present a polymer optical fiber (POF) Bragg grating (FBG) to measure liquid level based on Archimedes' law of buoyancy. The sensor consists of polymer 3D-printed rods with different radii attached to the fiber terminal containing an FBG. Characterization is performed by submerging the rods in a beaker containing water at different level heights. The tension force applied onto the optical fiber changes with the level of the liquid, which is then measured through the FBG. Considering the smaller Young's modulus of the POF compared to that of a silica optical fiber, it is possible to induce larger strain changes, and thus, enhance the liquid level sensitivity. Our results show a liquid level sensitivity enhancement of up to ≈ 21 times when compared to the silica FBG. This enhancement enables liquid level resolution of 0.2 mm for the polymer FBG as opposed to 2.6 mm for the silica counterpart.

1. Introduction

Nowadays, liquid level has been measured through various types of sensors [1]. Some examples include electrical [2,3], optical [4–6] and mechanical [7] sensor configurations. Liquid level measurement sparks particular interest due to the challenges of achieving consistency and security while maintaining precision. Thus, from the sensor categories reported earlier, the ones based on optical technologies ensure both features. Optical fiber sensors (OFSs) are a prime example in this category. OFS requires low power consumption, provide high precision, are safe because the materials composing the fibers are inert to most chemicals, and, due to their low power usage, they don't present the risk of igniting. Additionally, they can operate over long distances, are immune to electromagnetic interference, and are small and compact. These characteristics make them suitable for use in environments such as fuel reservoirs or public water reservoirs, which makes them preferable compared to their counterparts.

Liquid level OFSs have been reported through the use of long-period gratings (LPGs) [8], fiber Bragg gratings (FBGs) in silica [5,69] and polymer optical fibers (POFs) [10], multimode interferometers (MMIs)

[6], D-shape fibers [11], straight decladded fibers [12], bent side polished fibers [13], macro bending coupling [14], in-fiber micro holes [15], etc. However, critical parameters such as operating range, resolution, complexity and sensor reliability, are all difficult parameters to combine in a single sensor. For instance, the sensors based on D-shaped fibers [11], in-fiber micro holes [15], bent side polished fibers [13] and decladded fibers [12], present operating ranges that are restricted by the attenuation of the sensing regions, namely the polished regions, holes, bent regions or length of decladded region of the fibers. Additionally, their operating principle relies on optical power measurements as a consequence of the light refraction at the sensing regions, and thus, their response will differ for different solution's refractive index, and on top of that, their implementation in turbidity media is problematic, needing periodic washing of the sensing regions. This last problem is also shared by other liquid level OFSs as is the case of MMIs [6], LPGs [8] and etched fibers [9]. Moreover, intensity-based measurements are severely affected by source power fluctuation, but FBG based sensors do not. Among the OFS sensors reported so far, one that has received the most attention from the scientific community is the FBG. The reason is undoubtedly due to its simplicity and versatility. Despite that, the use of

* Corresponding author.

E-mail address: oliveiraricardo@ua.pt (R. Oliveira).

complex membrane arrangements [10] or cantilever systems makes their deployment difficult. To solve this, in 2018 Consales et al. [5] reported a simple FBG-based sensor working on the Buoyancy effect. This OFS consists of a cylinder rod of known mass and size attached to an FBG written in a glass optical fiber (GOF). In this sensor, the tension force acting on the FBG depends on the liquid level height, making the FBG able to respond with a measurable Bragg wavelength shift. The liquid level sensitivities reported in [5] were -3.8 and -7.0 pm/cm for rods with diameters of 3 and 4 mm, respectively. Thus, considering a wavelength resolution of 1 pm, the highest liquid level resolution would be ≈ 1.4 mm. However, the evaluation of this resolution depends on the area of the container. Thus, considering that large volumes require large container areas, a resolution of 1.4 mm could mean that several tens of liters are not taken into account. This could result in incorrect volume estimates and the possibility of leakages of hazardous liquid chemicals going unnoticed. Furthermore, when working with volatile liquids, this increases the likelihood of hazards. Thus, it is important to rapidly detect the presence of liquid leaks, allowing for the minimization of the risk of damage, ensuring environmental protection and natural resource conservation. One effective way to do that would be through the strain sensitivity enhancement of the OFS. Examples of this type of performance enhancement have already been explored for a strain sensor based on POFs in series with silica fibers, [16].

When compared to GOFs, POFs offer several interesting characteristics namely due to their lower Young's modulus (E), (≈ 2.2 – 3.4 GPa vs. ≈ 71.0 GPa), higher elastic limit (4.6 % vs. 0.6 %) [1718], higher flexibility, non-brittle nature, etc. Specifically, talking about the Young's modulus, a lower E means that for the same tension force, the POF will be subjected to a much higher strain than the GOF. Considering all these features and considering the OFS liquid level sensor based on Archimedes' law of Buoyancy, as reported in [5], it can be inferred that the FBG response would be enhanced if the GOF is replaced by a POF.

In this paper, we implemented POF Bragg grating sensors for liquid level measurement, based on Archimedes' law of Buoyancy. The performance between silica and polymer FBGs liquid level sensors will be analyzed analytically and experimentally allowing us to compare its performance in terms of sensitivity and resolution.

2. Operating principle

The OFS proposed in this work is based on the Archimedes' law of buoyancy. It consists of a 3D-printed rod of known dimensions and mass and is suspended by an optical fiber containing an FBG, as is shown in the schematic of Fig. 1.

As the liquid level height (H) inside the beaker changes, the strength of the forces that act on the rod also changes, thus, the strain on the FBG also changes. Consequently, the resonant Bragg wavelength will shift

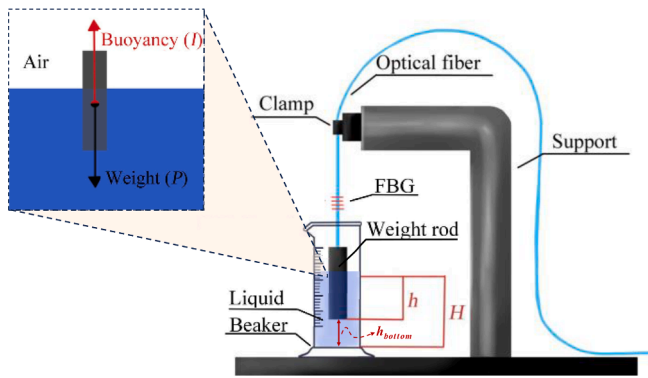


Fig. 1. Schematic of the liquid level sensor. A weight rod is suspended by an optical fiber containing an FBG and is immersed in a beaker containing liquid. The inset shows the forces acting on the rod, according to the Archimedes law of Buoyancy.

accordingly, and a proportional relationship between the Bragg wavelength shift ($\Delta\lambda_B$) and H can be established, which allows the measurement of the liquid level height.

In Fig. 1, two forces are acting on the rod, namely: the weight (P) and the buoyancy force (I). According to Archimedes' principle, the buoyancy force, defined as the upward force exerted on an object that is completely or partially submerged in a liquid, is equal to the weight of the liquid displaced by the submerged object. The volume of the displaced fluid is in turn, equal to the volume of the submerged portion of the object. By mathematically defining the force vectors and verifying the mentioned equivalence, we have:

$$\sum_{i=0}^N F_i = 0 \quad (1)$$

$$F = P - I \quad (2)$$

$$F = mg - I \quad (3)$$

$$F = mg - V_{subm}g\rho_{liq} \quad (4)$$

where F is the resulting tension force on the optical fiber, V_{subm} is the volume of the submerged portion of the object, m is its mass, g is the gravitational acceleration constant and ρ_{liq} the density of the liquid. In our work, the rod has the shape of a cylinder, and thus, its volume (V) is described as:

$$V = \pi r^2 h_{rod} \quad (5)$$

where r is the radius and h_{rod} is the height of the rod. For the volume of the submerged section of the rod, the equation is still the same, but the height (h) is now defined as the distance from the base of the cylinder up to the surface of the liquid level (Fig. 1). Thus, by replacing V_{subm} in Eq. (4), we obtain:

$$F = mg - \pi r^2 h g \rho_{liq} \quad (6)$$

The full description of the proposed sensor requires the demonstration of the relation between Eq. (6) and the FBG strain response with the inherent fiber mechanical properties.

According to the materials, the strain, ϵ , is given by:

$$\epsilon = \frac{\sigma_t}{E} \quad (7)$$

with σ_t being the tension and E the Young's modulus. Since the tension is related to the applied total force, Eq. (7) can be written as:

$$\epsilon = \frac{F}{AE} \quad (8)$$

where A is the cross-section area of the optical fiber in which the force is applied. By replacing F obtained in Eq. (6), into Eq. (8), we obtain:

$$\epsilon = \frac{g(m - \pi r^2 h \rho_{liq})}{AE} \quad (9)$$

To understand the effect that the strain has on the FBGs written on the fiber attached to the rod, let us define the Bragg wavelength (λ_B), according to the Bragg law:

$$\lambda_B = 2n_{eff}\Lambda \quad (10)$$

where n_{eff} is the effective refractive index of the optical fiber and Λ is the grating period [19]. Considering that the FBG is subjected to a change in longitudinal strain, a Bragg wavelength shift ($\Delta\lambda_B$) will be observed as described by:

$$\Delta\lambda_B = \lambda_B(1 - p_e)\epsilon \quad (11)$$

being p_e is the photo-elastic coefficient of the fiber [17]. By replacing Eq. (9) into Eq. (11), the following expression is obtained:

$$\Delta\lambda_B = \lambda_B(1 - p_e) \frac{g(m - \pi r^2 h \rho_{liq})}{AE} \quad (12)$$

This expression describes the Bragg wavelength shift response as the liquid level height changes.

Since H is the sum of h to the liquid height that exists between the bottom of the rod and the base of the liquid container (h_{bottom}), then, it is possible to rewrite the above equation as:

$$\Delta\lambda_B = \lambda_B(1 - p_e) \frac{g(m - \pi r^2 (H - h_{bottom}) \rho_{liq})}{AE} \quad (13)$$

3. Sensor fabrication

The experimental setup used in this work and depicted in Fig. 1, is composed of a metallic support bar, a weight rod suspended by an optical fiber containing an FBG, a fiber clamp to secure the fiber in a vertical position and a graduated beaker containing liquid water at room temperature. The rods were 3D printed with standard resin from Anycubic. We produced two rods with a height of 15 cm and radii of 3 and 4 mm. These two dimensions will be used to quantify the influence of the volume of the submerged object on the sensor's overall sensitivity. The GOF used in this work was a standard germanium doped single mode (SM) GOF, reference ITU G.652, distributed by Cabelte SA, shown in the inset of Fig. 2 (a). And the POF used in this work was a poly-methylmethacrylate (PMMA) microstructured polymer optical fiber (mPOF), doped with benzil dimethyl ketal (BDK). That was drawn at DTU Electro [20] and is composed of three rings of air holes with a diameter of 1.3 μm and pitch of $\approx 3.3 \mu\text{m}$, giving an air-filling fraction enough to guarantee endlessly single-mode operation (see picture at the inset of (b)).

Regarding the FBG sensor, it was fabricated through the phase mask method. For that, a focused laser beam of a 248 nm KrF, ultraviolet (UV)

pulsed laser was passed through a 572.12 nm phase mask, able to produce λ_B at the 850 nm region. The gratings were written with lengths of 4.8 mm and were fabricated with laser energy, repetition rate and a total number of pulses of 6 mJ, 500 Hz, and 5000 pulses for the GOF, and 2mJ, 1 Hz and 4 pulses for the mPOF. The difference in pulse energy, frequency, and number of pulses for each of the fibers was due to the different natures of the fibers. More information about this topic can be found in [17]. To interrogate the FBGs, light from an 850 nm broadband light source (Superlum SLD-371-HP1), was launched into one of the arms of a 50:50 ratio single-mode silica fiber optical coupler. The reflected spectrum was monitored with an OSA (Yokogawa AQ6317).

For the connection of the fiber to the 3D printed rod, it was used a small drop of a high tensile strength photopolymerisable resin (NOA86H, from Norland Inc.), with a tensile strength of 54 MPa, similar to that of the PMMA fiber. Regarding the FBG location, we placed it close to this connection (≈ 1 cm), however, we stress out that the location of the grating in the fiber is irrelevant, because the strain is homogeneously distributed along the length of the fiber, as a consequence of its constant A and E .

For the spectral monitoring of the FBG written in the mPOF, the terminal of a silica pigtail fiber was aligned and spliced through UV resin to the mPOF terminal [17,21,22]. The spectra measured after the grating inscription for the GOF and mPOF are shown in Fig. 2 (a) and (b), respectively.

These results show the presence of 3 and 1 Bragg peaks for the GOF and mPOF, respectively. The number of Bragg peaks present in each spectrum was due to the fibers' modal behavior in the 850 nm region. As the mPOF has an endlessly SM behavior, the presence of a single Bragg peak confirms the presence of one propagation mode. Concerning the GOF, its cutoff frequency is located at ≈ 1250 nm, thus, the presence of 3 Bragg peaks in the 850 nm region, indicates the presence of 3 propagation modes. As the fundamental mode propagates with a higher refractive index since it is more confined in the core central region, it is possible to infer through Eq. (10), that this mode will have a higher Bragg wavelength. This corresponds to the peak located further to the right side of the spectrum. Nevertheless, its high peak power compared to the remaining peaks also indicates that most of the power is transmitted in this mode. To allow for comparison between the studied fibers, only the Bragg peaks corresponding to the fundamental mode will be considered in the next subsections.

4. Liquid level measurement

The sensor was characterized by adding water into the beaker at regular intervals of 5 ml, corresponding to an increase in height of about 0.9 cm. This was done manually but carefully to minimize possible sources of error during the characterization. The obtained spectral results are shown in Fig. 3 (a) and (b), for the GOF and the mPOF, respectively.

As observed from Fig. 3, the Bragg peaks show a blue wavelength shift with the increasing liquid level height. This occurs because the fiber is subjected to less strain as the liquid height increases, which is in accordance with Eq. (12). To track the Bragg peak, we measured the wavelength at which the maximum occurs as shown by the black markers identified in Fig. 3. Then, we plotted the wavelength shifts as function of the liquid level height (h) as shown in Fig. 4 (a) and (b), for the 3 and 4 mm radius rods, respectively. In the same figures, it is also displayed the theoretical FBG wavelength shift responses calculated through Eq. (12). For that, we considered a liquid density of $\rho_{liq} = 1000$ kg/m³, gravitational acceleration of $g = 9.8$ m/s², rods' radii of $r = 3$ and 4 mm with a mass of 4.79 and 9.44 g, respectively, and finally, the fiber properties presented in Table 1.

The experimental results shown in Fig. 4 exhibit a linear behavior of $\Delta\lambda$ vs. h . Thus, a first-order linear regression model was applied to the experimental data and the corresponding sensitivities were obtained, reaching good correlations, with R^2 values close to one. The sensitivity

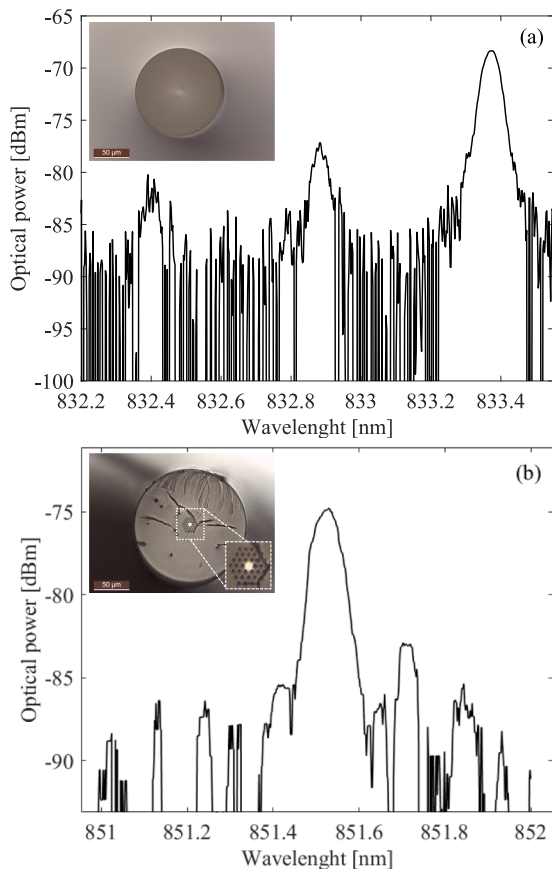


Fig. 2. Spectra of the FBGs at the 850 nm region, for the (a) GOF and (b) mPOF.

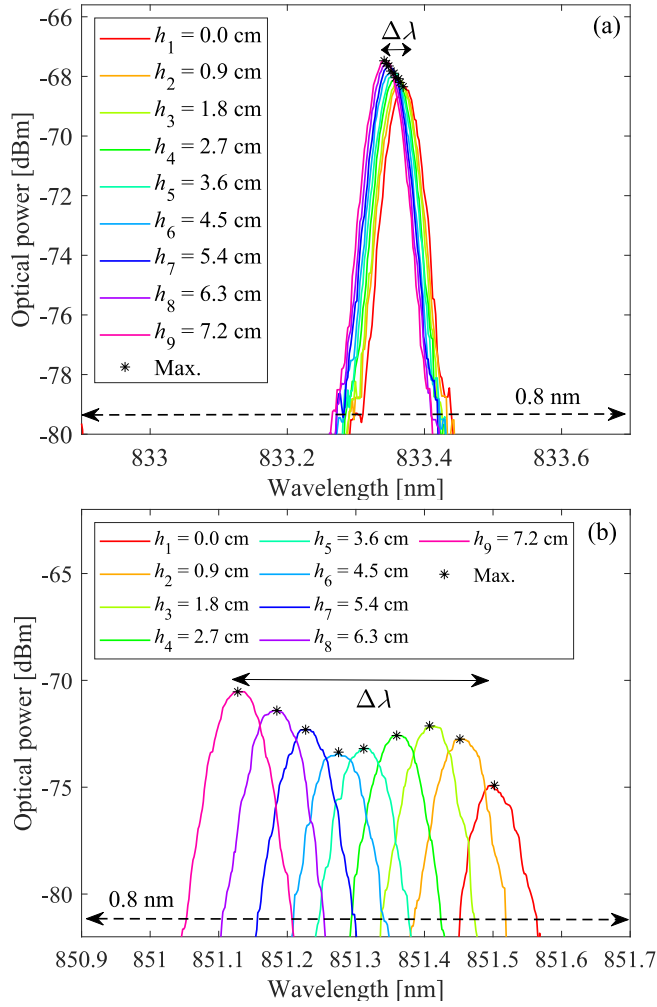


Fig. 3. Spectra measured for each liquid level height, using FBGs written in: (a) GOF, and (b) mPOF. All obtained for a 4 mm radius rod attached to the FBG.

results reached good linearities with maximum errors of 0.8 pm/cm for the mPOF-FBG characterized with a 4 mm radius rod. As observed, the experimental results are in agreement with the analytical calculations obtained from Eq.(12). An overview of the sensitivity results is shown in Table 2.

From Table 1, the similarities between the experimental and theoretical results are confirmed. Furthermore, the sensitivities reached for the 4 mm rod were higher than those obtained for the 3 mm. This is also in accordance with Eq. (12), where an increase in the radius of the rod, leads to an increase in the Bragg wavelength shift. While this analysis is important from the design point of view, the most important feature to take from the results presented in Fig. 4 and Table 1 is the higher sensitivities obtained for the mPOF compared to the GOF. Specifically, in the experimental results, we obtained a sensitivity of -28.7 vs. -1.6 pm/cm for the 3 mm rod and -51.4 vs. -3.8 pm/cm for the 4 mm rod, which corresponds to an improvement of up to 18 times. Again, from Eq. (12), it is possible to observe that a lower Young's modulus leads to a larger wavelength shift, so, a sensitivity improvement can be reached. From the same equation, it is also important to notice that the sensitivity is inversely proportional to the A of the fiber. Thus, considering that A of the mPOF is higher than that of the GOF, we are underestimating the liquid level sensitivity improvement. In theory, considering that the mPOF had the same area as that of the GOF, it would be possible to reach a theoretical sensitivity of 50.0 and 90.0 pm/cm for the 3 and 4 mm diameter rod, respectively, which could correspond to a liquid level sensitivity improvement of 24 times.

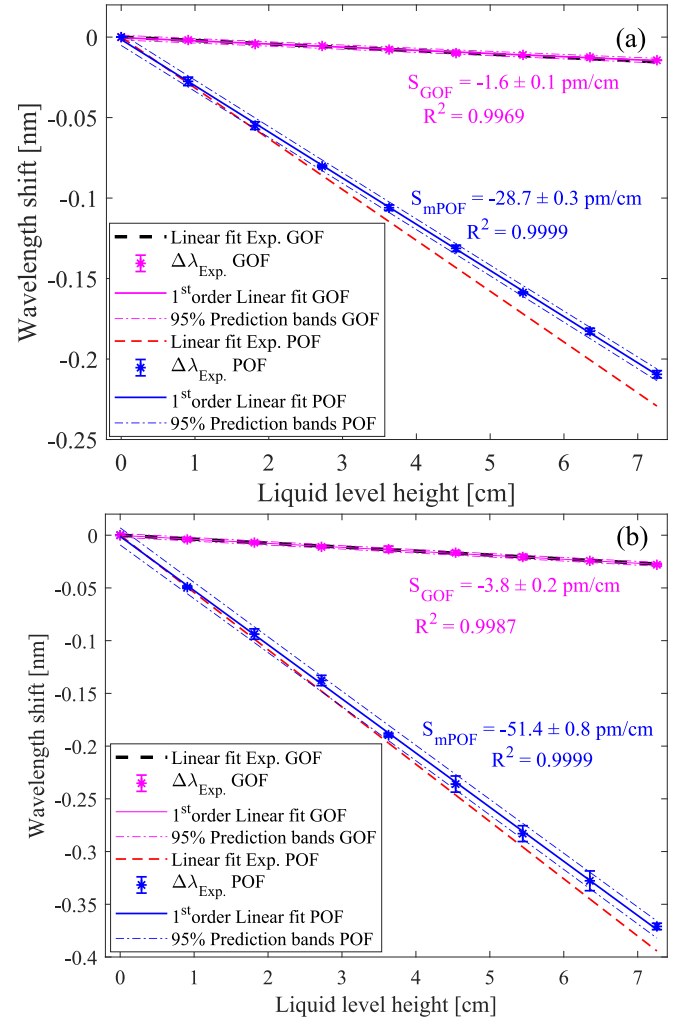


Fig. 4. Experimental and theoretical sensitivity curves for the (a) 3 mm and (b) 4 mm radii rod.

Table 1
Properties of the GOF and mPOF.

Parameter	GOF	mPOF
p_e	0o.204	0.0964
E (GPa)	31.1	3.4
r (μm)	62.5	80.0
A (m^2)	2.01×10^{-8}	$1.23 \times 10^{-8} \text{m}^2$

Table 2
Theoretical and experimental liquid level sensitivities.

Rod radius (mm)	Fiber	$S_{\text{The.}}$ (pm/cm)	$S_{\text{Exp.}}$ (pm/cm)	Res. (mm)
3	GOF	-2.1	-1.6 ± 0.1	6.3 ± 0.4
	mPOF	-31.1	-28.7 ± 0.3	0.348 ± 0.004
4	GOF	-3.7	-3.8 ± 0.2	2.6 ± 0.1
	mPOF	-55.4	-51.4 ± 0.8	0.195 ± 0.003

Using a common detection system with a 1 pm resolution, our mPOF-FBG sensor is able to obtain a liquid level resolution of 0.348 ± 0.004 and 0.195 ± 0.003 mm for the 3 and 4 mm radii rods, respectively. This is a much higher resolution than the one obtained for the GOF, which was 6.3 ± 0.4 and 2.6 ± 0.1 mm, respectively. Consales' team achieved a resolution of 2.6 and 1.4 mm for the 3 and 4 mm rods with a GOF containing FBG at the 1550 nm region [5]. These results are different

and higher than the results achieved in this work for the GOF. However, the Bragg wavelength of the sensor reported in [5] is 700 nm higher than the one reported in this work. Thus, according to Eq. (12), the longer the wavelength the higher the sensitivity. The results presented in this work for both mPOF and GOF were shown for shorter wavelengths, i.e. 850 nm. The reason was due to the high PMMA attenuation at 1550 nm ($\approx 1\text{--}3$ dB/cm [17]). Changing the sensor interrogation window from 850 nm to 1550 nm allows to enhance the liquid level sensitivity by a factor of ≈ 2 . Taking into account the low attenuation of CYTOP POFs at 1550 nm [23], it would be interesting to develop the POF-FBG liquid level sensor at this wavelength region. However, even working at lower wavelengths, our mPOF FBG sensor still shows better liquid level resolution performance than that reported by Consales and co-workers at the 1550 nm region, i.e., 0.2 mm vs. 1.4 mm, (7 times higher). Overall, the sensor presented in this work behaves very well when compared to the ones reported in literature, as is seen in Table 3. Also, it allows to solve some of the disadvantages reported by other works as detailed in the introduction section and compiled here in this table.

The liquid level height tested in this work was only 7.2 cm, however, this is not even close to the liquid height limit of the proposed sensor. In fact, the liquid level height limit of our sensor as well as the ones reported in [5] and [24], depends only on the strength of the fiber used. Thus, this is dependent on the rod mass and on the mechanical strength of the fiber used. Considering the polymer material used in this work with a tensile strength of ≈ 100 MPa, this would result in a maximum theoretical liquid level height of several tens of centimeters.

Regarding the liquid level resolution, the sensor configuration tested in this work achieves one of the highest resolutions. Furthermore, it is worth noting that the sensitivity of the sensor could still be further enhanced if the setup considers the OFS secured in the two fiber ends and with the weight rod sitting at the fiber sensor middle region as was described by Paul et al. [24]. The configurations of each of the reported

sensors, namely by Consales et al. [5], Paul et al. [24], and ours are schematized in Fig. 5 for easy comprehension.

Through the configuration shown in the left of Fig. 5, and reported in [24], it is possible to observe a “ $2 \cdot \sin(\theta)$ ” term on the denominator of the wavelength shift equation response. Where θ corresponds to the angle formed by the fiber when compared to its straight configuration. Thus, by proper adjustment of θ , namely, to reach the smallest value, it is possible to enhance the sensitivity by several times. Paul et al. were able to set θ up to 8° and this allowed them to reach a sensitivity enhancement of $1/(2 \times \sin(8^\circ)) \approx 3.6$ times compared to the configuration of Consales et al. By replacing the GOF with the POF, we enhanced the sensitivity by a factor of ≈ 21 times, which is considerably better. However, we stress that the combination of the Paul et al. configuration and the use of POF instead of GOF, can improve even more the performance of the sensor presented in this work, (i.e., 3.4 times). To take a better picture of the theoretical sensitivity enhancement for each of the configurations, we considered optical fibers with the same diameter (125 μm), FBGs located at 850 nm wavelength, rod with 4 mm radius and 9.44 g and finally $\theta = 8^\circ$ for the sensor configuration based on two anchoring parts as was used in Paul’s work. From that, we may estimate the theoretical sensor responses as shown in Fig. 6.

From Fig. 6 it can be concluded that the use of the POF together with the fixation of it in two points, allows an increase of the sensitivity by a factor of 75 times compared to the GOF with a single anchored region. This would allow to measure the liquid level height with a resolution of 0.03 mm. This clearly indicates that the synergetic effect of the use of POF as proposed in this work, with the use of two anchoring points as proposed by Paul et al., can be used to boost even more the result reached in this work. In order to make a full comparison of the different type of sensors, it is shown in Table 4, the compilation of the sensitivity values and resolution of the Archimedes’ law of buoyancy sensors consisting of similar parameters for a fair comparison.

The in-field deployment of the proposed sensor requires compact packaging of all the parts used for the spectral interrogation of the liquid-level sensor. For this purpose, compact on-the-shelf interrogators working at the 850 nm region may be used. Regarding the sensor installation and packaging, we need to take into account that the sensor deals with mobile parts. In this way, we recommend packaging the POF attached to the rod inside a perforated hollow tube. This would give robustness to the sensor and make it easier to manipulate and install. For easy visualization of the proposed in-filed sensor application, we added a schematic of it in Fig. 7.

The practical scenario presented in Fig. 7 or even other possible scenarios require experimental tests on the topic. Examples could involve testing the sensor in various liquids with different densities, temperatures, and levels of turbulence to assess its accuracy and reliability under real-world conditions. However, such works reinforce the importance of those in future practical scenarios for the actual application of the sensor.

Spectrally interrogated sensors as the liquid level sensor proposed in this work, do always require capital investment. However, optical power detection techniques, such as the use of edge filtering techniques [6] can be used to allow the wavelength shift of an FBG to be measured as an optical power quantity, capable of being measured through a photodetector. While this has not been the strategy followed in this work, this approach could be used to reduce the cost of the sensor in a perspective of market deployment.

Polymers contrary to silica, are known to absorb small quantities of water from the environment. While one could replace the polymer rod by a metal rod and the PMMA POF by and humidity-insensitive POFs [25], fouling of substances to the rod or POF could still impact the long-term stability of the sensor and its accuracy. Thus, for a long-term sensor application, a thin hydrophobic spray coating based on fluorinated compounds can be applied to both POF and 3D printed polymer rod, making the sensor immune to the water absorption, chemically more resistant and foulant free.

Table 3
Liquid level heights and sensitivities of different works.

Sensor Type	Fiber type	Liquid level height (cm)	Sens.	Res. (mm)	Disadvantages
D-shaped POF [11]	POF	18	1.2 %/mm	1.00	Limited range due to attenuation &
Decladded POF [12]	POF	55	1.4 mV/mm	0.21	Affected by the liquid refractive index and turbidity
Side polished POF [13]	POF	39	0.08 dB/mm	2.20	
Macrobending POF [14]	POF	35	1.4 nW/mm	0.07	
Hole on POF [15]	POF	40	5e-4 %/mm	50.00	
Tapered GOF [9]	GOF	2.4	2.56 dB/mm	0.04	Affected by the liquid refractive index and turbidity
LPG + GOF [8]	GOF	100	–	200.00	
FBG + MMI + GOF [6]	GOF	5.2	0.25 dB/mm	0.08	
Diaphragm + POF + FBG [10]	POF	75	57.3 pm/cm	0.17	Needs to adapt the reservoir
Archimedes + GOF + FBG [5]	GOF	25	27 pm/cm	0.37	<u>Ease of Breakage + low E</u>
Archimedes + GOF + FBG [24]	GOF	30	71.6 pm/cm	0.14	
<u>Archimedes + POF + FBG (This work)</u>	POF	7.2	51.4 pm/cm	0.19	–

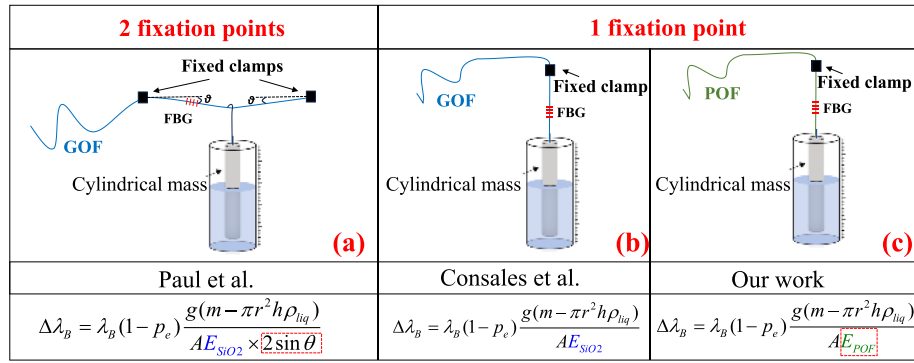


Fig. 5. Schematic of the configurations used in different works, considering GOF sensors with (a) two [24] and (b) one [5] fixed terminals, and with (c) POF fixed with one terminal. The corresponding wavelength shift equations are also shown at the bottom of each configuration.

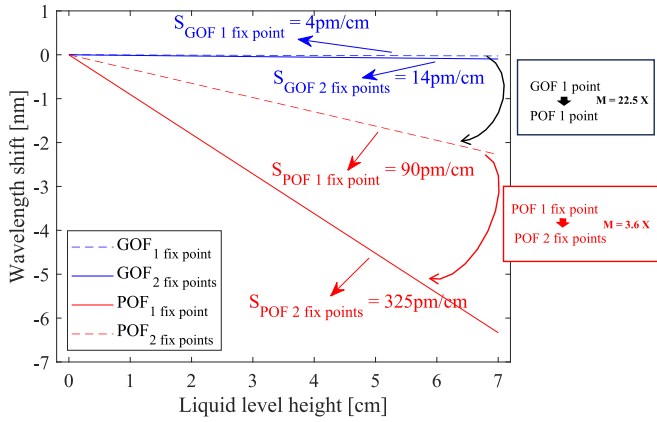


Fig. 6. Analytical response of the sensor configurations presented in Fig. 5, for a fiber with 125 μm diameter, FBGs at 850 nm, 8° angle for the configuration with 2 fixation points, and for a rod with 4 mm radius and 9.44 g.

Table 4

Comparison of the sensors performance considering the sensors based on the Archimedes' law of buoyancy presented in Fig. 5, for a fiber with 125 μm diameter, FBGs at 850 nm, 8° angle for the configuration with 2 fixation points, a rod with 4 mm radius and 9.44 g and, a 1 pm resolution detector.

Technology	Fiber	Fixation points	$ S_{The.} $ (pm/cm)	Res. (mm)
Consales et al. [5]	GOF	1	4	2.50
Paul et al. [24]	GOF	2	14	0.71
Ours	POF	1	90	0.11
Proposed	POF	2	325	0.03

As is observed in Eq. (12), the density of the liquid affects the sensor response. Thus, for liquids other than water, i.e., with different densities, it is necessary to readjust the sensitivity curve of the sensor. For that, it is required to know the liquid being used, or in other words, its density, ρ_{liq} . Then, the sensitivity obtained in this work for the water (S_{H_2O}), should be corrected to the sensitivity of the liquid under study (S_{liq}). Therefore, through simple proportion, it is possible to write the sensitivity of the new liquid as, $S_{liq} = (\rho_{liq}/\rho_{H_2O}) * S_{H_2O}$, where ρ_{H_2O} , is the water density. Through this, it would be possible to swap the sensor for different liquids without compromising its response.

FBGs also respond to temperature changes, and this can pose cross-sensitivity issues to the proposed liquid level sensor. Thus, for uncontrolled temperature environments, a possible solution could be done through the use of an in-series FBG that can measure the Bragg wavelength shift associated with the temperature variations, and then, subtract this wavelength shift to the Bragg wavelength response of the FBG liquid level sensor.

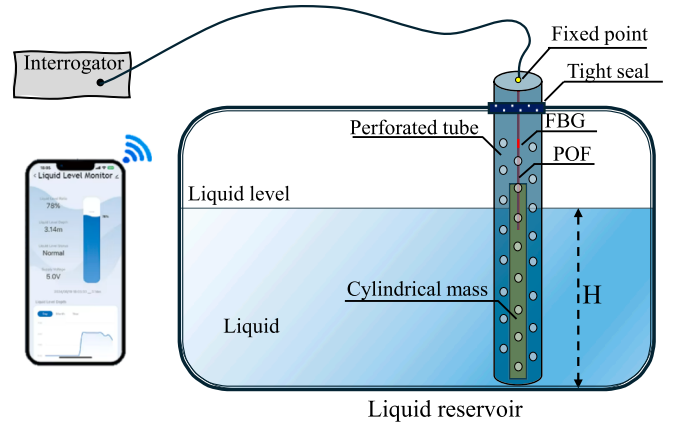


Fig. 7. Schematic of the proposed in-field liquid level sensor.

Furthermore, it is known that temperature influences the density of the liquid. Thus, the performance of the sensor can be compromised. However, this can be solved by knowing the density-temperature relationship of the liquid under study. Through that and using the FBG temperature sensor to measure the actual temperature, it would be possible to do a real-time estimate of the liquid density and with that, perform a real-time correction to the sensitivity curve. This would allow to make the sensor immune to the fluctuation of ρ due to temperature changes. While temperature and density issues could be potentially solved, it is worth to mention that high liquid turbulence could lead to instabilities to the sensor measurement scheme. While the packaging solution proposed in Fig. 7 could minimize the problem, we emphasize that the sensor is more adequate for non-turbulent media.

5. Conclusion

In this work, we fabricated a liquid level sensor based on Archimedes' law of buoyancy, using either GOF- or mPOF-FBGs attached to weight rods of different radii. This approach allowed us to compare the performance of both OFS in terms of sensitivity and resolution. The analytical and experimental characterization results demonstrated an improved liquid level response for larger rods and, more importantly, for fibers with a lower Young's modulus, as is the case for the mPOF (i.e., $E_{POF} = 3.4$ GPa vs. $E_{GOF} = 71.0$ GPa). This resulted in a sensitivity improvement of 18 to 14 times higher, for the 3 and 4 mm rods, respectively, compared to the GOF. Considering a detection system with 1 pm resolution, this sensitivity enhancement allows for an improvement in liquid level resolution from 2.6 to 0.2 mm, simply by changing the optical fiber type. Consequently, using an mPOF could potentially enable the detection of small leakages in large liquid reservoirs, such as

industrial tanks, chemical processing plants, water reservoirs for environmental monitoring and flood management. This minimizes the risk of damage, ensuring environmental protection and the conservation of natural resources.

CRedit authorship contribution statement

Cláudio C. Ramos: Writing – review & editing. **João Preizal:** Writing – review & editing, Investigation. **Xuehao Hu:** Writing – review & editing, Visualization, Resources. **Christophe Caucheteur:** Writing – review & editing. **Getinet Woyessa:** Writing – review & editing. **Ole Bang:** Writing – review & editing. **Ana M. Rocha:** Writing – review & editing. **Ricardo Oliveira:** Writing – review & editing, Validation, Supervision, Methodology, Investigation, Funding acquisition, Conceptualization.

Declaration of competing interest

The authors declare that they have no known competing financial interests or personal relationships that could have appeared to influence the work reported in this paper.

Acknowledgement

This work was supported by FCT - Fundação para a Ciência e Tecnologia, I.P. by project reference UIDB/50008, and DOI identifier 10.54499/UIDB/50008 and by FCT/MEC under the project (PTDC/EEI-TEL/1511/2020). R. Oliveira acknowledges the FCT contract CEE-CIND2021.01066. The Fonds de la Recherche Scientifique (F.R.S.-FNRS) under the Postdoctoral Researcher grant (Chargé de Recherches) of Xuehao Hu and the Research Director Position of Christophe Caucheteur.

Data availability

Data will be made available on request.

References

- [1] K. Loizou, E. Koutroulis, Water level sensing: State of the art review and performance evaluation of a low-cost measurement system, *Meas. J. Int. Meas. Confed.* 89 (2016) 204–214, <https://doi.org/10.1016/j.measurement.2016.04.019>.
- [2] S.J. Moon, Y.L. Han, S.H. Hwang, S.J. Kang, J.M. Lee, B.S. Bae, Integrated water-level sensor using thin-film transistor technology, *ACS Omega* 8 (2023) 36868–36875, <https://doi.org/10.1021/acsomega.3c03914>.
- [3] A. Kodavatiganti, Water Level Monitoring, *Int. J. Res. Eng. Appl. Sci.* 8 (2018) 1–5. <https://ssrn.com/abstract=3292084>.
- [4] A.M. Pozo, F. Pérez-Ocón, O. Rabaza, A continuous liquid-level sensor for fuel tanks based on surface plasmon resonance, *Sensors* 16 (2016), <https://doi.org/10.3390/s16050724>.
- [5] M. Consales, S. Principe, A. Iele, M. Leone, H. Zaraket, I. Jomaa, A. Cutolo, A. Cusano, A fiber Bragg grating liquid level sensor based on the archimedes' law of buoyancy, *J. Light. Technol.* 36 (2018) 4936–4941, <https://doi.org/10.1109/JLT.2018.2866130>.
- [6] R. Oliveira, S. Aristilde, J.H. Osório, M.A.R. Franco, L. Bilro, R.N. Nogueira, C.M. B. Cordeiro, Intensity liquid level sensor based on multimode interference and fiber Bragg grating, *Meas. Sci. Technol.* 27 (2016) 125104, <https://doi.org/10.1088/0957-0233/27/12/125104>.
- [7] A. Kulkarni, R.N. Karekar, R.C. Aiyer, Liquid level sensor, *Rev. Sci. Instrum.* 76 (2005) 105108, <https://doi.org/10.1063/1.2054412>.
- [8] J.-N. Wang, C.-Y. Luo, Long-period fiber grating sensors for the measurement of liquid level and fluid-flow velocity, *Sensors* 12 (2012) 4578–4593, <https://doi.org/10.3390/s120404578>.
- [9] B. Yun, N. Chen, Y. Cui, Highly sensitive liquid-level sensor based on etched fiber bragg grating, *IEEE Photonics Technol. Lett.* 19 (2007) 1747–1749, <https://doi.org/10.1109/LPT.2007.905093>.
- [10] C.A.F. Marques, G. Peng, D.J. Webb, Highly sensitive liquid level monitoring system utilizing polymer fiber Bragg gratings, *Opt. Express* 23 (2015) 6058–6072.
- [11] S.M. Chandani, N.A.F. Jaeger, Optical fiber-based liquid level sensor, *Opt. Eng.* 46 (2007) 114401–114406, <https://doi.org/10.1117/1.2801506>.
- [12] A.S. Rajamani, D. M. V.V.R. Sai, Plastic fiber optic sensor for continuous liquid level monitoring, *Sensors Actuators, A Phys.* 296 (2019) 192–199. Doi: 10.1016/j.sna.2019.07.021.
- [13] M. Lomer, A. Quintela, M. López-Amo, J. Zubia, J.M. López-Higuera, A quasi-distributed level sensor based on a bent side-polished plastic optical fibre cable, *Meas. Sci. Technol.* 18 (2007) 2261–2267, <https://doi.org/10.1088/0957-0233/18/7/061>.
- [14] H. Zhang, L. Feng, Y. Hou, S. Su, W. Liu, J. Liu, J. Xiong, Optical fiber liquid level sensor based on macro-bending coupling, *Opt. Fiber Technol.* 24 (2015) 135–139, <https://doi.org/10.1016/j.yofte.2015.05.012>.
- [15] J. Park, Y.J. Park, J.D. Shin, Plastic optical fiber sensor based on in-fiber microholes for level measurement, *Jpn. J. Appl. Phys.* 54 (2015) 2–5, <https://doi.org/10.7567/JJAP.54.028002>.
- [16] R. Oliveira, T.H.R. Marques, C.M.B. Cordeiro, R. Nogueira, Strain Sensitivity Enhancement of a Sensing Head Based on ZEONEX Polymer FBG in Series With Silica Fiber, *J. Light. Technol.* 36 (2018) 5106–5112, <https://doi.org/10.1109/JLT.2018.2870054>.
- [17] R. Oliveira, L. Bilro, R. Nogueira, *Polymer Optical Fiber Bragg Gratings: Fabrication and Sensing Applications*, CRC Press, Boca Raton (2019), <https://doi.org/10.1201/9780367822705>.
- [18] G. Woyessa, O. Bang, Recent advances on speciality polymer optical fibres for bragg grating sensors, in: 30th Int. Conf. Plast. Opt. Fibers, Bilbao (Spain), 2023.
- [19] K.O. Hill, G. Meltz, Fiber Bragg grating technology fundamentals and overview, *J. Light. Technol.* 15 (1997) 1263–1276, <https://doi.org/10.1109/50.618320>.
- [20] X. Hu, G. Woyessa, D. Kinet, J. Janting, K. Nielsen, O. Bang, C. Caucheteur, BDK-doped core microstructured PMMA optical fiber for effective Bragg grating photo-inscription, *Opt. Lett.* 42 (2017) 2209–2212, <https://doi.org/10.1364/OL.42.002209>.
- [21] S.D. Carson, R.A. Salazar, Splicing Plastic Optical Fibers, in: M. Kitazawa, J.F. Kreidl, R.E. Steele (Eds.), *Plast. Opt. Fibers*, SPIE Proceedings, Boston, 1991: pp. 134–138. Doi: 10.1117/12.51000.
- [22] X. Yue, H. Qu, R. Min, G. Woyessa, O. Bang, X. Hu, Convenient connectorization technique between single mode polymer optical fiber and single mode silica optical fiber, Eighth Symp. Nov. Photoelectron. Detect. Technol. Appl. 12169 (2022) 1216974, <https://doi.org/10.1117/12.2624940>.
- [23] Y.-G. Nan, D. Kinet, K. Chah, I. Chapalo, C. Caucheteur, P. Mégret, Ultra-fast fiber Bragg grating inscription in CYTOP polymer optical fibers using phase mask and 400 nm femtosecond laser, *Opt. Express* 29 (2021) 25824–25835, <https://doi.org/10.1364/oe.428592>.
- [24] D. Paul, S.K. Khijwania, Highly Sensitive and Temperature Insensitive Fiber Bragg Grating Based Liquid-Level Sensor, in: Proc. - 28th Int. Conf. Opt. Fiber Sensors, OFS 2023, Optica Publishing Group, 2023: p. W4.100. Doi: 10.1364/OFS.2023.W4.100.
- [25] W. Yuan, L. Khan, D.J. Webb, K. Kalli, H.K. Rasmussen, A. Stefani, O. Bang, Humidity insensitive TOPAS polymer fiber Bragg grating sensor, *Opt. Express* 19 (2011) 19731–19739, <http://www.ncbi.nlm.nih.gov/pubmed/21996915>.